Effects of Porosity, Fiber Size, and Layering Sequence on Sound Absorption Performance of Needle-Punched Nonwovens

Nazire Deniz Yilmaz,[1] Pamela Banks-Lee,[2] Nancy B. Powell,[2] Stephen Michielsen[2]

[1]*Department of Textile Engineering, Pamukkale University, Denizli, Turkey*
[2]*College of Textiles, North Carolina State University, Raleigh, North Carolina*

Received 20 April 2010; accepted 1 September 2010
DOI 10.1002/app.33312
Published online 31 March 2011 in Wiley Online Library (wileyonlinelibrary.com).

ABSTRACT: The relationships between the material parameters, i.e., the fiber fineness, porosity, areal density, layering sequence, and airflow resistivity with the normal-incidence sound absorption coefficient of nonwoven composites consisting of three layers have been studied. The monofiber or multifiber needle-punched nonwovens included poly(lactic acid) (PLA), polypropylene (PP), glass fiber, and hemp fibers. Air flow resistivity was statistically modeled and was found to increase with decreasing fiber size and nonwoven porosity. The former models developed for glass fiber mats in the literature were found to be inconsistent with the air flow resistance of the nonwovens reported below. The effects of the layering sequence on air flow resistivity and sound absorption were obtained. It was found that when the layer including reinforcement fibers, i.e., hemp or glass fiber, faced the air flow/sound source, the air flow resistance and the absorption coefficient were higher than the case when the layer including reinforcement fibers was farthest from the air flow/sound source. The difference was more pronounced if there was a greater difference between the resistivity values of the constituent layers of the nonwoven composite. Sound absorption coefficient was statistically modeled in terms of air flow resistivity and frequency. © 2011 Wiley Periodicals, Inc. J Appl Polym Sci 121: 3056–3069, 2011

Key words: airflow resistivity; sound absorption; fibers; biodegradable; renewable resources

INTRODUCTION

Noise, once ignored as an irritating but harmless nuisance,[1] is now considered to be a major public health concern. Noise has countless negative effects, which include hearing loss, hypertension, cardiac disease, ulcers, colitis, headache, nausea, dizziness, insomnia, annoyance, fear, and stress.[2] Noise can also decrease performance in various working environments.[1] To give an example, the unwanted sound present in the passenger cabin of a vehicle diminishes speech intelligibility, exhausts the driver, and affects safety negatively.[3]

There are three major methods to reduce unwanted noise: modify noise- and vibration-emitting sources, use barriers to prevent sound propagation, and dissipate sound energy with the use of sound absorption materials.[4] Sound absorbers are porous materials where the sound is attenuated in tortuous channels of pores present in the material.[5] Absorbers are classified in three groups: cellular materials (e.g., foams), granular materials (e.g., woodchip panels), and fibrous materials.[6]

Nonwoven fabrics, classified as fibrous sound absorbers, have important potential in noise reduction applications. Nonwovens offer advantages over foams as they can be recycled and their manufacturing methods may have less environmental impact than conventional polyurethane sound absorbers.[7] Nonwovens can also absorb more sound over a wider range of frequencies compared with foams.[8]

Sound absorption is mostly due to acoustic energy dissipation resulting from the viscosity and heat conductivity of medium in the porous material. Air flow resistivity, porosity, and tortuosity have been cited as the main factors that affect sound absorption by several researchers.[9,10]

Air flow resistivity is among the most important parameters influencing the sound absorption performance of porous absorbers.[9,10] Delany and Bazley[11] used air flow resistivity as the main material variable to model sound absorption. Besides acoustical performance,[6] air flow resistivity is of prime importance in terms of the fibrous structure's filtration,[12] barrier,[13] and comfort properties.[14]

Correspondence to: Nazire DenizYilmaz (ndyilmaz@pau.edu.tr or ndyilmaz@ncsu.edu).

Contract grant sponsors: Scholarship for Doctoral Research and Education at North Carolina State University from Turkish Council of Higher Education (to N.D.Y.).

According to ASTM C522-03 Standard Test Method for Airflow Resistance of Acoustical Materials,[15] the flow resistance, R, has units of mks acoustic ohm (Pa s m^{-3}). It is obtained when the pressure drop across a specimen is divided by the volume velocity of airflow through the specimen. Specific flow resistance, r, with the unit of mks rayls (Pa s m^{-1}), is obtained when the flow resistance of a specimen is multiplied by its area. It is equivalent to the pressure difference across the specimen divided by the linear velocity of flow measured outside the specimen. Flow resistivity, r_0, in mks rayl/m (Pa s m^{-2}), of a homogeneous material, is obtained when its specific flow resistance is divided by its thickness. The flow resistance, R, the specific flow resistance, r, and the flow resistivity, r_0, of porous materials can be given by the following equations:

$$R = \frac{p}{u} \tag{1}$$

$$r = \frac{p \cdot S}{u} \tag{2}$$

$$r_0 = \frac{p \cdot S}{l \cdot u} \tag{3}$$

where R is the flow resistance, r is the specific flow resistance, r_0 is the flow resistivity, p is the pressure drop across the sample in Pa, S is the area in m^2, l is the thickness in m of the porous material, and u is the volumetric velocity of the fluid in m^3/s. Despite the fact that all these terms are valid only for steady flow, and not for oscillatory flow as in the case for sound waves,[9] they have been adopted by the majority of researchers for the sake of simplicity.

For homogeneous materials, the specific flow resistance is linearly related to the material thickness. Thus, the flow resistivity, which is specific flow resistance divided by the thickness, is a characteristic of the material, independent of thickness.[16]

Air flow resistivity is closely related to the density of a nonwoven web. Flow resistivity increases with increasing density. Ballagh[17] developed the following formula for woolen nonwovens:

$$r_0 = k\rho_w^{1.61} \tag{4}$$

where r_0 is the flow resistivity in mks rayl/m (Pa s m^{-2}), ρ_w is the density of web in kg m^{-3}, and k has the value of 16 with the unit of Pa s $m^{2.83}$ $kg^{-1.61}$.

The flow resistivity is reported to be proportional to the reciprocal of the square of the pore size of the material when the microstructure is considered. Thus, in fibrous materials, decreasing the fiber diameter increases the flow resistivity.[18] However, the fiber type affects the relationship between the fiber size and the flow resistivity.[8] Porosity, tortuosity,[19] mean pore size, pore size distribution,[12] fiber orientation,[20] and fabric surface characteristics[21] influence flow resistivity in addition to the fabric density and fiber diameter

Until now, glass fiber mats have been the focus of research and modeling efforts on sound absorption characteristics and air flow resistivity[6] among fibrous absorbers. Nonwoven fabrics may be a viable alternative to glass fiber mats with their lower specific densities, their ability to be recycled, and their flexibility in material selection, which allows the use of natural fibers and engineered biodegradable polymer fibers.

In this study, air flow resistivity and sound absorption of three-layered nonwoven composites consisting of single and multiple types of fibers were reported. These nonwoven composites included conventional fibers such as polypropylene (PP) fibers and glass fibers, and engineered biodegradable polymer fibers such as poly(lactic acid) (PLA) fibers and natural fibers such as hemp fibers. The effects of fiber size, porosity, and sequencing of the constituent layers on air flow resistivity and sound absorption were investigated.

EXPERIMENTAL

Materials

Four different fiber types were used in nonwoven production, and scanning electron microscopy (SEM) images of them are shown in Figure 1. The types and the functions of the selected fibers are given in Table I, and their properties are given in Table II. PLA fibers were donated by Fiber Innovation Technology (Johnson City, TN). Cardable glass fiber was donated by AGY Holding Corp (Aiken, SC), and PP fibers were donated by the Nonwovens Cooperative Research Center (Raleigh, NC). Hemp used in this research was obtained from Stemergy (ON, Canada). Hemp was field retted and processed through BioFibeRefinery™ technology of Stemergy. Hemp was selected as the natural fiber in this research because it is a strong, stiff biodegradable fiber type based on renewable resources, which has characteristics comparable with flax fibers but less studied. Under normal conditions, hemp has 6–12% moisture ratio, 310–750 MPa tensile strength, and 30–70 GPa tensile modulus.[22–25]

Sample preparation

Nonwoven fabric production involved three steps: fiber opening, web formation, and web bonding. The fibers, which were supplied in dense press-packed bales, were opened in a Truetzschler Opener. All fiber webs were produced in single-fiber web form except for one sample set, which included 33% glass

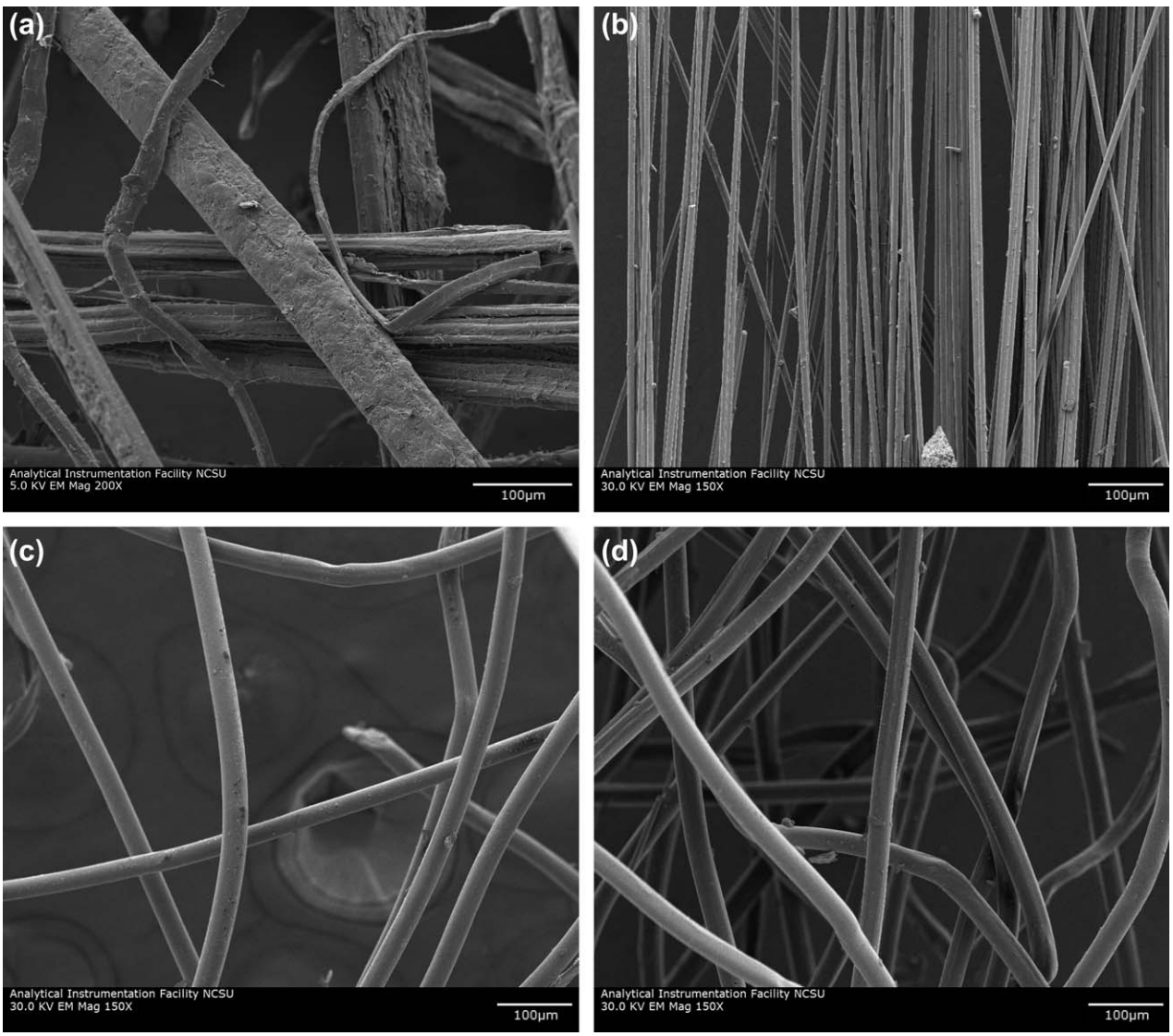

Figure 1 SEM images of fibers (a) hemp, (b) glass fiber, (c) PLA, and (d) PP at 30.0 kV. The magnification of hemp fiber (×200) is different from the other fibers (×150).

fiber and 66% PP as shown in Table III. Blending for this sample was carried out by loading the fibers of the two different types into the Truetzschler Opener.

An air laying method was used for the web forming step. In this method, fibers that were fed into an air stream were transferred to a perforated drum or

TABLE I
Types and Functions of Selected Fibers

Fiber group	Function	Layer code	Fiber type	Reason for selection
I	Provides mechanical reinforcement to the nonwoven composite	R1	Hemp	Biodegradable; replaces glass fiber in conventional automotive nonwoven composites
		R3	Glass fiber	Commonly used in automotive nonwoven composites
II	Carrier in nonwovens; provides moldability and processability	C1	PLA	Biodegradable; to replace PP in conventional automotive nonwoven composites
		C2	PP	Commonly used in automotive nonwoven composites; recyclable
I + II	Mixture of the mechanical reinforcement and carrier groups from conventional fibers	M2	Glass fiber/ PP (33/67)	Defining the effect of blending before web bonding

TABLE II
Fiber Parameters

Fiber	Structure	Length (cm)	Void ratio (%)	Fiber radius (10^{-6} m) Mean	σ	Fiber density (10^{-3} kg m^{-3})	Apparent fiber density (10^{-3} kg m^{-3})
PLA	Hollow	6.4	18	30.9	3.1	1.24	1.02
PP	Solid	5.1	N.A.	31.7	1.3	0.91	0.91
Glass fiber[a]	Solid	5.1	N.A.	9.00	0.74	2.50	2.50
Glass fiber[b]	Solid	5.1	N.A.	10.9	0.82	2.50	2.50
Hemp	Multifibrillar	5.1	N.A.	42	38	1.45	1.45

[a] Glass fiber in layered PP/glass fiber/PP blend.
[b] Glass fiber in intimate polypropylene-glass fiber blend.

moving belt where the fiber web was formed. Truetzschler Tuft Feeder Scanfeed was used for air laying with a target basis weight of 330 gsm (grams per square meter). The webs formed are listed in Table III. After air laying, webs were preneedled using a NSC Asselin Preneedler.

The formed webs had little strength and had to be bonded by some means. Needle-punching was used for web bonding. Before needle-punching, three layers of webs from either the same or different fibers were stacked as given in Table IV. Even though single fiber type nonwoven fabric samples from all four fibers were planned to be studied; only samples of 100% PLA and 100% PP were successfully fabricated. Attempts at producing 100% hemp and 100% glass fiber nonwovens failed because lack of cohesion among fibers. Figure 2 gives a general production flow chart, in which A, B, and C are given in Table IV. In the stacks of web layers, carrier fibers were used at a higher percentage compared with reinforcement fibers to provide moldability for the resulting fabric.

In needle-punching, the perforation of the webs by specially designed needles caused fiber entanglement. Three-layered webs were needled on a NSC Asselin needle-punch loom set at a 100 cm/min speed, 100-cm width, with needles on both sides, 228 strokes/cm, 175 punches/cm^2 penetration density, and 3 mm penetration depth. Groz-Beckert 15 × 17 × 40 × 3 needles were used. A target of 1000 gsm (g m^{-2}) basis mass was set. Compositions of nonwoven fabrics produced using needle punching are given in Table IV.

Characterization

Fibers were characterized based on fiber diameter. Fabrics were characterized in terms of mass per unit area, thickness, porosity, and air flow resistivity. Samples were subjected to conditioning at 20°C and 65% relative humidity for at least 24 h before characterization.

Fiber linear density

Average diameters of all fibers were determined using ASTM D 1577-07 Standard Test Methods for Linear Density of Textile Fibers.[26] Average linear densities of the fibers were obtained by fiber diameter measurements on SEM images. A Hitachi S-3200N scanning electron microscope at the Analytical Instrumentation Facility of North Carolina State University was used. A 4Pi EDS/Digital Imaging system was used to acquire SEM digital images and line scans. At least 30 specimens of hemp fibers and 10 specimens of man-made fibers were measured.

Fabric mass per unit area

Mass per unit area values of fabric samples were measured in accordance with ASTM D 3776-07 Standard Test Method for Mass Per Unit Area (Weight) of Fabric.[27] Five samples with a minimum diameter of 8.89 cm (3.5 in.) were cut randomly and weighed in grams using a Mettler Toledo Precision Weighing (AG 245) balance. When the basis weight results obtained were thought to be inconsistent with sound absorption results, the sound absorption specimens were weighed. Sound absorption specimens, which were circular with a diameter of 29 mm, had smaller dimensions than required by the standard ASTM D 3776-07.

TABLE III
Fiber Webs Produced by Truetzschler Tuft Feeder Scanfeed

Web numbers	Layer codes	Fiber composition of webs	Blend ratios (%)
1	R1	Hemp	100
2	C1	PLA	100
3	C2	PP	100
4	R3	Glass fiber	100
5	M2	Glass fiber/PP	33/67

TABLE IV
Layering of Fiber Webs before Needle-Punching

Web number	Web code	Layer codes	Layer 1 (A)	Layer 2 (B)	Layer 3 (C)
1	HLL	R1/C1/C1	Hemp	PLA	PLA
2	LHL	C1/R1/C1	PLA	Hemp	PLA
3	LLH	C1/C1/R1	PLA	PLA	Hemp
4	LLL	C1/C1/C1	PLA	PLA	PLA
5	HPP	R1/C2/C2	Hemp	PP	PP
6	PHP	C2/R1/C2	PP	Hemp	PP
7	PPH	C2/C2/R1	PP	PP	Hemp
8	PPP	C2/C2/C2	PP	PP	PP
9	GPP	R3/C2/C2	Glass fiber	PP	PP
10	PGP	C2/R3/C2	PP	Glass fiber	PP
11	PPG	C2/C2/R3	PP	PP	Glass fiber
12	PGI	M2/M2/M2	Glass fiber/PP	Glass fiber/PP	Glass fiber/PP

Thickness

At least five thickness measurements were taken from each sample using an AMES thickness gauge with pressure level 4.14 kPa according to ASTM D 5729-97 Standard Test Method for Thickness of Nonwoven Fabrics.[28]

Porosity

Porosity values of five specimens of all nonwoven samples were calculated according to ASTM C 830-00 Standard Test Methods for Apparent Porosity, Liquid Absorption, Apparent Specific Gravity, and Bulk Density of Refractory Shapes by Vacuum Pressure[29] using eq. (5):

$$h = 1 - \frac{\rho_w}{\rho_f} \tag{5}$$

where h is porosity, ρ_w is the density of the fabric, and ρ_f is the density of the fiber.

Airflow resistivity

Air flow resistivity of nonwoven webs was determined according to ASTM D 737-04 Standard Test Method for Air Permeability of Textile Fabrics.[30] The Frazier air permeability tester (Frazier Precision Instrument Company Inc.) was used to test five specimens of each sample. The Frazier Differential Pressure Air Permeability Instrument gave the rate of flow of air in cubic feet per square foot of sample area per minute, the Frazier Number, at a differential pressure of 0.5 in. of water.[31] These units have been converted to air flow resistivity, r_0, in Pa s m^{-2} as shown in eq. (3), where l is the thickness of the fabric in meters (equation derived from Frazier[27] and ASTM D 737-04[30]):

$$r_o = \frac{0.5 \times 249}{\text{Frazier\_Number} \times 0.00508 \times l} \tag{6}$$

Sound absorption coefficient

The impedance tube method was used to determine the normal-incidence sound absorption coefficient (NAC). A minimum of three specimens of each sample were tested according to ASTM E 1050-07 Standard Test Method for Impedance and Absorption of Acoustical Materials Using a Tube, Two Microphones and a Digital Frequency Analysis System.[32] A Bruel & Kjaer Pulse™ acoustic material

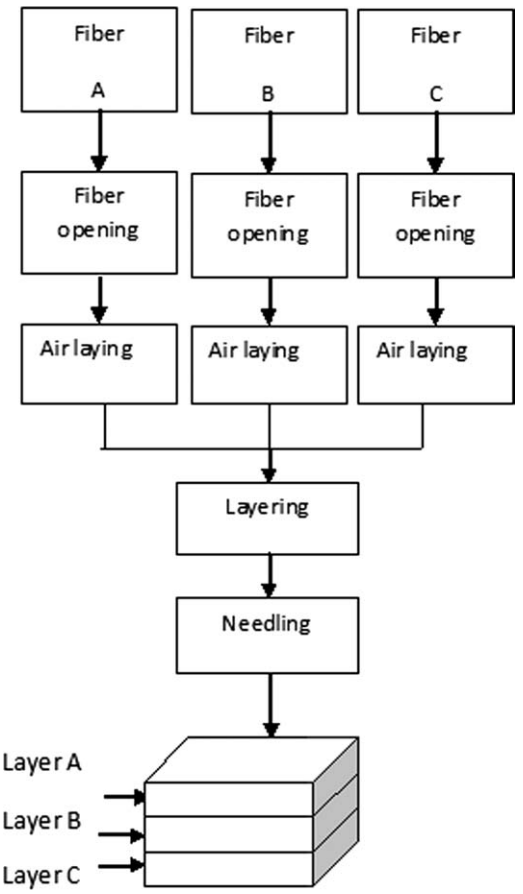

Figure 2 General production flow chart.

Figure 3 Bruel & Kjaer two-microphone impedance tube type 4206.[33]

testing system, which included a type 4206 two-microphone impedance tube, shown in Figure 3, a Pulse™ Type 3560 multichannel portable data acquisition unit, and Pulse TM type 7758 software, were used at Carcoustics Tech Center. A 29-mm-diameter tube was used, and the frequency range analyzed was 500–6400 Hz.

A schematic diagram of the acoustical material testing system is given in Figure 4. The impedance tube was composed of a hollow cylinder, a sound source at one end, and a test sample holder at the other. At two locations along the wall of the tube, microphone ports were mounted. The working principle for sound absorption testing is as follows: Broadband plane sound waves are formed in the tube with the help of a sound source. A stationary wave pattern is generated in the tube. This stationary wave pattern is composed of the incident sound and the reflected sound. The incident and the reflected/not absorbed components of the wave pattern are analyzed with simultaneous pressure measurements at two locations in the tube. A digital frequency analysis system determines the NAC as a function of sound frequency. NAC is measured according to eq. (7):

$$\alpha_n = 1 - |Я|^2, \tag{7}$$

where α_n is NAC, and $Я$ is the reflection coefficient.[4]

RESULTS AND DISCUSSION

As described in the Introduction section, porosity, h, has a major effect on acoustical properties. It appears as a direct coefficient in fundamental wave equations, with only connected pores are taken into consideration for predicting air flow resistivity.[9]

Effect of porosity on airflow resistivity: Analysis on monofiber nonwovens

PPP fabric had a significantly higher basis weight and lower porosity than LLL fabrics as shown in Table V. The mean air flow resistivity of PPP fabric was about 30% higher than the LLL fabric as well.

A number of empirical models in the literature have been used to describe the effect of material parameters on air flow resistivity. These include models for glass fiber mats by Bies and Hansen,[34] glass fiber mats with different fiber orientations by Sullivan (in Mechel[20]), for polyester mats by Garai and Pompoli,[35] as reported in Cox and D'Antonio,[8] and for wool mats by Ballagh.[17] All of the models, except for those of Ballagh[17] and Garai and Pompoli,[35] gave values significantly lower than those measured in this study, as seen in Table VI. The reason for this may be that the structures studied by Garai and Pompoli[35] and by Ballagh[17] were similar to the ones studied here. Ballagh[17] and Garai and Pompoli[35] also attributed the lack of agreement between their models and those of the other authors as being due to the difference in the fiber radii between glass fibers and the other types of fibers studied.

Garai and Pompoli's[35] and Ballagh's[17] models were corrected with the ratio of the density of the fiber of the model to the density of each fiber in this research to obtain the real porosity as given in Table VI. Ballagh's model gave the closest values to the mean measured air flow resistivity. In both

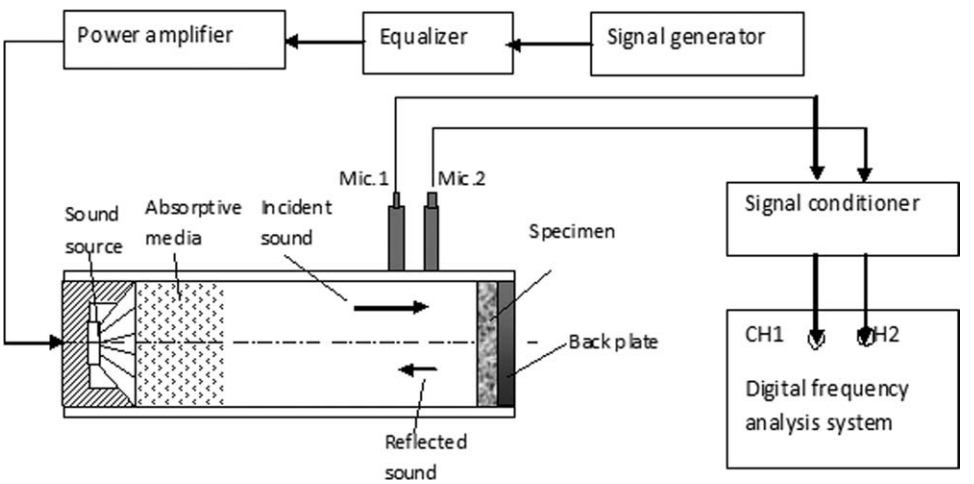

Figure 4 Schematic diagram of acoustical material testing system (adapted from ASTM E 1050-08[32] and Bruel & Kjaer[33]).

TABLE V
Air Flow Resistivity and Structure Parameter Information of Single-Fiber Type Webs

	Basis weight (kg m^{-2})		Thickness (mm)		Porosity $1 - \rho_w/\rho_f$		Air flow resistivity (10^3 Pa s/m^2)	
Fabric	Mean	σ	Mean	σ	Mean	σ	Mean	σ
LLL	1.13	0.12	12.22	0.24	0.91	0.01	23.4	1.4
PPP	1.37	0.07	12.45	0.33	0.88	0.01	30.0	3.2

LLL, PLA/PLA/PLA; PPP, PP/PP/PP.

Garai and Pompoli's[35] and Ballagh's[17] models, only the density of the fabric and the diameter of the fiber were included. Because Ballagh[17] only used one type of fiber in his research, the density of the fabrics gave enough information to determine the porosity. However, as there are two different fibers with different densities in the current analysis, the massivity variable, which is the ratio of fabric density to fiber density, or porosity subtracted from unity, has been used instead of just the density of fabrics. The PLA fibers used in this research had a hollow structure. However, the voids in PLA were assumed to be unconnected pores and not included in porosity. Thus, PLA fibers were assumed to act like solid fibers in terms of air resistivity. The fiber density for PLA fibers had to be corrected for their void fraction. This was accomplished by multiplying the fiber density by (1.00–0.18), as the void fraction of the PLA fibers is 0.18.

As there was only approximately 3% difference between the radii of PLA and PP fibers, the fiber radii are assumed to be the same, and the fiber radius was not included in the model as a variable at this point. The air flow resistance was fit according to eq. (8).

$$r_0 = A + B\frac{\rho_w^{1.6}}{\rho_f^{1.6}} \tag{8}$$

where r_0 is air flow resistivity in mks rayl/m, ρ_w is the density of web, and ρ_f is the density of the fiber in kg m^{-3}. In the generated statistical model shown in eq. (8), $A = 16{,}400$ mks rayl/m and $B = 367{,}000$ mks rayl/m. The model had a coefficient of determination (R^2) value of 0.46. The reason for the low R^2 value might be the high variation in the samples and the low number of data points. The fitting of

TABLE VI
Air Flow Resistivity Values of PLA and PP Fabrics: Actual Average and Semi-Empirical Model Predictions

Air flow resistivity (Pa s m^{-2})			
LLL	PPP	Model	Explanation
23,410	30,000	N/A	Average measured value
2,580	4,410	$r_0 = 27.3(1-h)^{1.53}(\mu/4a^2)$	Glass fiber (Bies and Hansen[34])
2,200	3,840	$r_0 = \left\{3.94\mu(1-h)^{1.413}\left[1+27(1-h)^3\right]\right\}/a^2h$	Glass fibers parallel to flow, single fiber radii (Sullivan, as reported in Mechel[20])
5,930	10,500	$r_0 = \frac{6.8\mu(1-h)^{1.296}}{a^2h^3}$	Glass fibers perpendicular to flow, single fiber radii, $20 \le a \le 30$ μm (Sullivan, as reported in Mechel[20])
2,310	4,330	$r_0 = \frac{4\mu}{a^2}\left[\frac{0.55(1-h)^{4/3}}{h} + \frac{\sqrt{2}(1-h)^2}{h^3}\right]$	Glass fibers, random fiber orientation, single fiber radii (Sullivan, as reported in Mechel[20])
1,570	2,570	$r_0 = 3.2\mu(1-h)^{1.42}/a^2$	Glass fibers, random fiber distribution, random fiber radius distribution (Sullivan, as reported in Mechel[20])
1,430	2,490	$r_0 = 4.4\mu(1-h)^{1.59}/a^2$	Mineral fiber, random fiber distribution, random fiber radius distribution, (Sullivan, as reported in Mechel[20])
8,240	12,120	$r_0 = 28.3\rho_W^{1.404}/(4\cdot 10^{12}a^2)$	Polyester fibers (Garai and Pompoli[35])
15,300	22,500	$r_0 = 28.3\left(\rho_W\frac{\rho_{PET}}{\rho_f}\right)^{1.404}/(4\cdot 10^{12}a^2)$	Corrected by the ratio of polyester fiber density to the density of fiber of interest (modified Garai and Pompoli[35] equation)
18,170	26,600	$r_0 = 490\rho_W^{1.61}/10^6a$	Wool fibers (Ballagh[17])
15,620	39,230	$r_0 = \left[490\left(\rho_W\cdot\rho_{wool}\Big/\rho_f\right)^{1.61}\right]/10^6a$	Corrected by the ratio of wool fiber density to the density of fiber of interest (modified Ballagh[17] equation)

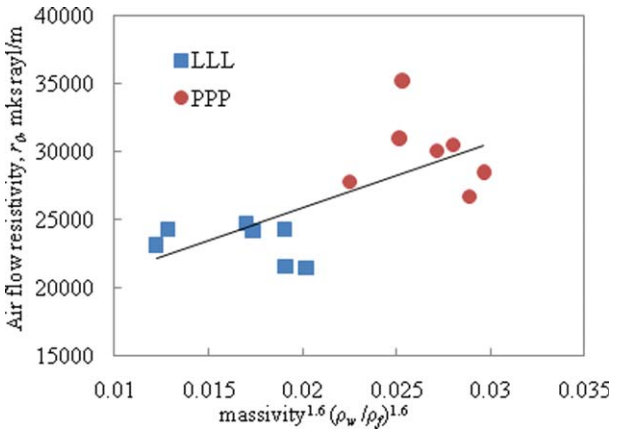

Figure 5 Comparison of statistical model estimates versus actual values for air flow resistivity values of single-fiber nonwoven fabrics as determined from eq. (8). [Color figure can be viewed in the online issue, which is available at wileyonlinelibrary.com.]

the model versus the actual values is shown in Figure 5. However, it should be noted that the effect of porosity was confounded with the effect of fiber type and fiber length. Because no mention to the effect of fiber length on the air flow resistance has been found in the literature, the 25% length difference between PLA and PP fibers were ignored. Nonwovens of same fabric type with different porosities should be investigated in terms of air flow resistivity to obtain a more accurate model.

Effect of fiber fineness: Analysis on mono- and multifiber nonwovens

Three-layered single fiber polypropylene (PPP) and PLA (LLL) fabrics were compared with three-layered PP-glass fiber (66/33), intimate blend (PGI), and three-layered PP/glass fiber/PP fabrics (PGP) to detect the effect of fiber size on air flow resistivity. The air flow resistivity information of PGP and PGI composites are given in Table VII. As seen from Tables II and VIII, glass fiber had a smaller fiber radius than the PLA and PP fibers. To obtain the effective fiber size of the multifiber fabrics, a weighted average of fiber radius was calculated based on the percentage of the number of each type of fiber. The percentages of number of the fibers were found using eq. (9):

$$\frac{N_i}{N_T} = \frac{\frac{m_i/m_T}{\rho_i \times a_i^2}}{\frac{m_i/m_T}{\rho_i \times a_i^2} + \frac{m_j/m_T}{\rho_j \times a_j^2}} \tag{9}$$

where N_i/N_T is the ratio of the number of the fiber of interest to the total number of fibers, ρ_i is the density, and m_i/m_T is the ratio of the mass of the fiber of interest in the web to the total fiber mass. The subscript "j" stands for the other fiber. The effective fiber radii of fabrics were calculated as follows:

$$\tilde{a}^2 = \frac{N_i}{N_T} a_i^2 + \frac{N_j}{N_T} a_j^2, \tag{10}$$

where $\tilde{a}$ is the weighted root mean square fiber diameter of the fabric. Among the various ways of averaging fiber diameter considered, eq. (10) has been found to be the optimum in terms of accuracy and practicality. The weighted average fiber density, $\hat{\rho}$, of the multifiber materials was calculated based on the volume fraction each fiber occupies to the total polymer material volume, as shown in eq. (11). Unlike PGI, PGP had layers of different materials. Nevertheless, both are treated as homogeneous material with the use of weighted average fiber diameter and density.

$$\hat{\rho} = \frac{m_T \rho_i \rho_j}{\rho_i m_j + \rho_j m_i} \tag{11}$$

where $\hat{\rho}$ is the weighted average fiber density of the multifiber nonwoven fabric. Equation (8) was modified to account for the weighted fiber radii, which resulted in eq. (12). For eq. (12), $A = 12{,}400$ mks raly/m and $B = 5.23 \times 10^{-4}$ mks rayl/m. The coefficient of determination, R^2 was 0.90. Figure 6 shows the air resistivity data along with the fit to eq. (12). No prominent difference is observed between the trends of the single fiber and multifiber fabrics at this point. However, it should be noted that the effects of fiber diameter and porosity are confounded with different fiber types and composite layouts. Thus, a fixed polymer system with different porosities and

TABLE VII
Air Flow Resistivity and Structure Parameter Information of Multifiber Type Webs

	Basis weight (kg m^{-2})		Thickness (mm)		Porosity $(1 - \rho_w/\rho_f)$		Air flow resistivity (10^3 Pa s/m^2)	
Fabric	Mean	σ	Mean	σ	Mean	σ	Mean	σ
PGP	1.44	0.13	12.4	0.17	0.90	0.01	47.8	4.2
PGI	1.49	0.14	13.1	0.64	0.91	0.01	46.3	3.93

PGP, PP/glass fiber/PP; PGI, PP-glass fiber intimate blend fabrics.

TABLE VIII
Weighted Average Fiber Diameters and Fiber Densities of PP/Glass Fiber/PP Layered and PP-Glass Fiber Intimate Blend Fabrics

Fabric	Weight (%)		Number fraction of fibers (%)		Volume fraction of fibers (%)		Fiber radius (10^{-6} m)		Weighted average density (10^{-3} kg m^{-3})	Weighted average fiber radius (10^{-6} m)
	PP	Glass	PP	Glass	PP	Glass	PP	Glass		
PGP	66	34	32	68	85	15	31.5	9.00	1.15	16.3
PGI	66	34	32	68	85	15	31.5	10.9	1.15	17.6

fiber diameters should be studied for further research.

$$r_0 = A + B\frac{\rho_w^{1.6}}{\rho_f^{1.6} \times \tilde{a}^2} \tag{12}$$

Effect of porosity on NAC (monofiber analysis)

In the frequency range 500–6300 Hz, PPP fabrics had generally higher NAC values than LLL as seen in Figure 7. Interestingly, PPP had higher variability for frequencies lower than 2.5 kHz and lower variability in frequency range above that level compared with LLL as shown in Table IX. Fibrous porous materials tend to have lower variability in region where minimum or maximum absorption takes place. As seen from Table IX, the increase and decrease in the coefficient of variation of PPP absorption was followed by those of LLL. The difference between the variability of the two fabrics implies that the absorption curve of PPP fabric was shifted to the left, i.e., lower frequency, compared with LLL. As seen from Table VI, PPP had higher air flow resistivity compared with LLL. These findings agree with those reported by Bies and Hansen,[16] who reported that greater air flow resistivity led to lower frequency sound absorption.

To investigate the effect of material parameters on NAC, air flow resistivity, and thickness, which have been accepted as the most important factors on NAC by many researchers, have been selected for statistical modeling along with frequency. The model below has been generated for the analysis of PPP and LLL fabrics.

$$\alpha_n = \sin\left(-2.61 \times 10^{-1} + 2.37 \times 10^{-4} f + 8.27 \times 10^{-6} r_0\right), \tag{13}$$

where α_n is the NAC, f is frequency in Hz, and r_0 is air flow resistivity in mks rayl/m. A high coefficient of determination, 0.97, was obtained partly due to the overwhelming effect of frequency. The thickness parameter was not found to be important in the model, possibly because of the narrow range of the thicknesses: ~ 12–13 mm. The model estimates are compared with our measured data in Figure 8.

Effect of hemp fiber on airflow resistivity

PHP and LHL fabrics, which contained hemp fibers, were added to the model eq. (12) are shown in Figure 9. The fiber weighted root-mean-square diameter and weighted average of fiber density for LHL and PHP are given in Table X.

The inclusion of hemp-containing nonwoven fabrics decreased the coefficient of determination despite the increase in population size. Fabrics containing hemp fiber showed a different trend than the

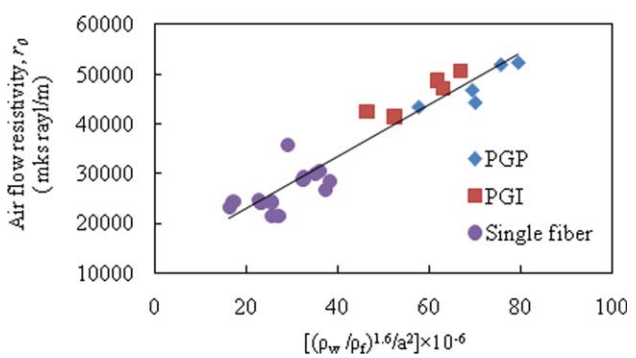

Figure 6 The air flow resistivity is plotted against eq. (12) for single-fiber nonwoven fabrics and multifiber PP/glass fiber/PP layered and PP-glass fiber intimated blend fabrics. [Color figure can be viewed in the online issue, which is available at wileyonlinelibrary.com.]

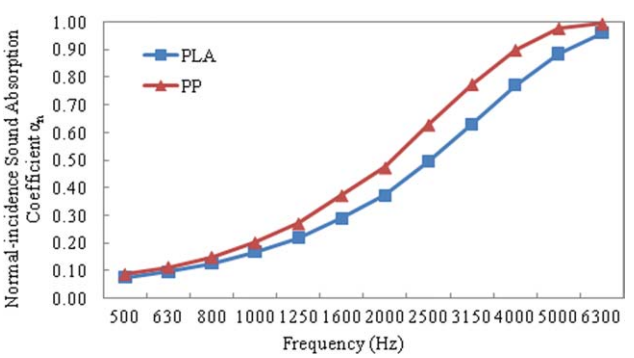

Figure 7 Comparison of averages of NAC values of LLL and PPP. [Color figure can be viewed in the online issue, which is available at wileyonlinelibrary.com.]

TABLE IX
NAC Information of Three-Layered LLL (PLA) and PPP (PP) Fabrics

	Normal-incidence sound absorption coefficient					
	Mean (μ)		Standard deviation (σ)		Coefficient of variation (%)	
Frequency	PLA	PP	PLA	PP	PLA	PP
500	0.08	0.09	0.004	0.007	5.52	8.53
630	0.10	0.11	0.005	0.010	5.22	8.52
800	0.13	0.15	0.006	0.012	5.00	8.24
1000	0.17	0.20	0.009	0.018	5.28	8.72
1250	0.22	0.27	0.013	0.024	6.18	8.89
1600	0.29	0.37	0.019	0.031	6.61	8.45
2000	0.37	0.47	0.033	0.043	8.92	9.09
2500	0.49	0.63	0.041	0.031	8.21	4.99
3150	0.63	0.78	0.048	0.029	7.57	3.68
4000	0.77	0.90	0.052	0.021	6.68	2.34
5000	0.88	0.98	0.047	0.008	5.30	0.81
6300	0.96	0.99	0.033	0.004	3.45	0.40

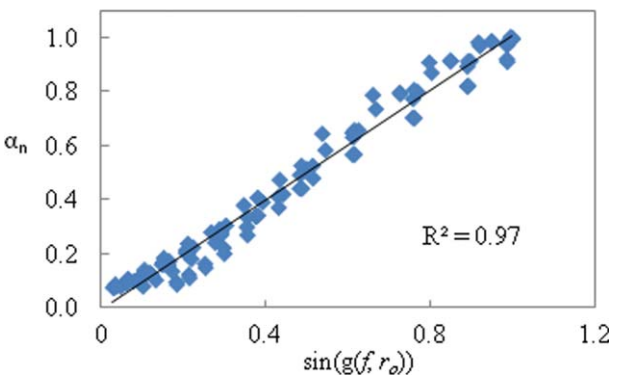

Figure 8 Comparison of statistical model estimates versus actual values for NAC values of PLA and PP fabrics. X-axis is a function of frequency and air flow resistivity. [Color figure can be viewed in the online issue, which is available at wileyonlinelibrary.com.]

others as seen in Figure 9. However, as the variation was high and nonuniform, and the sample size was small, no interpretations should be made at the moment. The curve in hemp containing fabrics may be due to the high variation in measured fabric parameters. The other reason may be the irregular

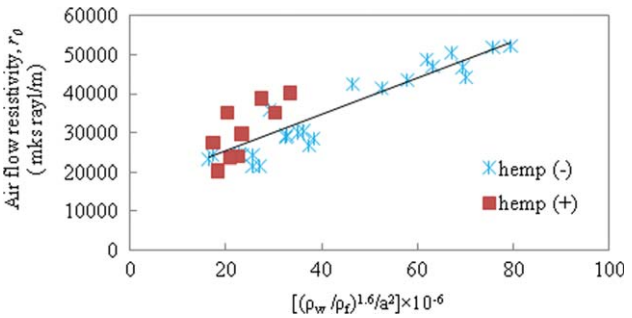

Figure 9 Comparison of statistical model estimates versus actual values for air flow resistivity values of single-fiber, and multifiber PP/glass fiber/PP layered, PP-glass fiber intimated blend, PLA/hemp/PLA and PP/hemp/PP fabrics. Fabrics that contain hemp and those do not are shown separately. [Color figure can be viewed in the online issue, which is available at wileyonlinelibrary.com.]

shape of hemp fibers as shown in Figure 10. The high irregularity of hemp fibers' cross-sections might have led to an increase in the surface area and tortuosity, which, in turn, increased the air flow resistivity. The moisture content present in the hydrophilic hemp fiber was not expected to have an effect because humidity is significant only for large distances.[9] This area needs more investigation with a greater sample size.

Effect of layering on air flow resistivity

The effect of layer sequencing on air flow resistivity was measured with three different placements of the reinforcement fiber layer, i.e., hemp or glass fiber layer, in the composite "sandwich" structure. These three different positions of the reinforcement layer were front side (closest to the air flow source), back side (furthest away from it), or in the middle, as shown in Table IV. The fabrics where the reinforcement was nearest to (front side) or farthest away (back side) from the air flow source in fact were the same fabrics, just flipped to the other side for air flow permeability and NAC testing. The material

TABLE X
Weighted Average Fiber Diameters and Fiber Densities of PLA/Hemp/PLA and PP/Hemp/PP Layered Fabrics

	Weight (%)		Number fraction of fibers (%)		Volume fraction of fibers (%)		Fiber radius (10^{-6} m)		Weighted average density (10^{-3} kg m^{-3})	Weighted average fiber radius (10^{-6} m)
Fabric	Carrier[a]	Hemp	Carrier	Hemp	Carrier	Hemp	Carrier	Hemp		
LHL	66	34	85	15	25	75	30.9	42.	1.13	32.8
PHP	66	34	84	16	23	77	31.5	42.	1.04	33.3

[a]Carrier web refers to PLA for LHL fabrics, and PP for PHP fabrics.

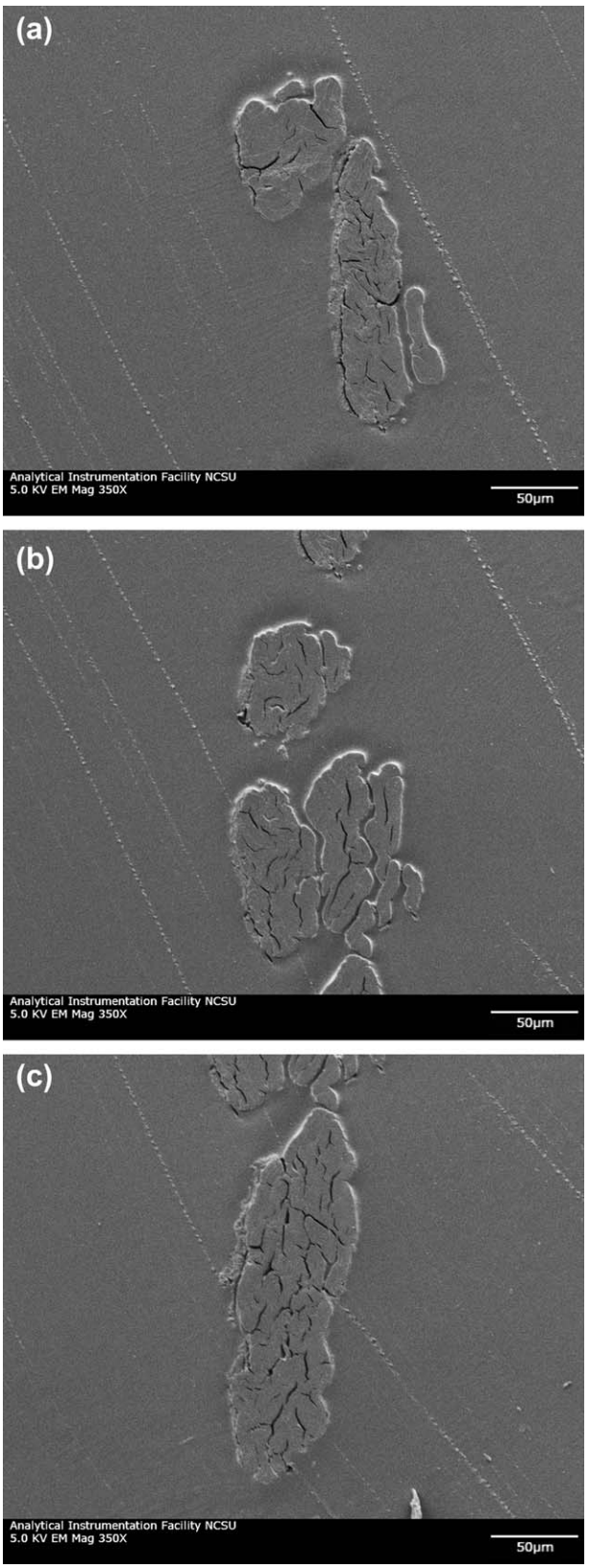

Figure 10 SEM images of hemp fiber cross-sections embedded in epoxy (5.0 kV; magnification, ×350).

parameters of the fabrics with different layer sequencing are given in Table XI.

No significant effects of layer sequencing were found with random readings from the fabrics with three different sequencings. This could be due to high variation of the fabrics. A paired *t*-test was run to look for a possible effect of layer sequence for the samples where the reinforcement fiber layer is either in the front or in the back side (GPP versus PPG, HLL versus LLH, and HPP versus PPH. The first letter stands for the layer that faces the air flow and the last letter for the layer at the back side). For all the measurements, when the layer of reinforcement fibers was in the front side (GPP, HLL, and HPP) the fabrics gave higher air flow resistivity than when it was on the back side as shown in Figure 11(a–c), respectively. This might be due to the higher reflectivity at the air-nonwoven boundary in the case of higher resistivity of the reinforcement layer compared with carrier layers, i.e., PLA and PP. The difference was more pronounced for GPP and PPG as presented in Table XII. This might be because the diameters of the glass fibers were less than one third of PP fibers' diameters; thus, the glass fiber mat should have had a higher resistivity. This means the average air flow in the glass fiber layer was slower than it was in the PP layer, which was already slower than the flow in unconstrained air. Therefore, the difference between the air flow resistivity values in the glass fiber layer and free air was greater than it was between the PP layer and free air. This leads to the fact that the interface between free air and the glass fiber layer produced more reflectivity than the interface between free air and the PP layer.

Although HPP and HLL had statistically higher air flow resistivity values than those of PPH and LLH respectively, the difference was small. This suggests that the hemp layer had slightly higher resistivity than both PP and PLA layers. Although the average diameter of hemp was slightly higher than those of PLA and PP, the high variation in fiber diameter and the irregular shape of hemp fibers might have led to higher tortuous path to air flow through the fabric layer. This is in accordance with Figure 10.

Effect of layer sequencing on NAC

Similar to the modeling of single-fiber webs, only air flow resistivity and frequency were found to be significant factors that affect NAC. The narrow range of thickness, which was approximately 11–13 mm, was thought to prevent the thickness variable to be included into the model. The statistical model shown in eq. (14) was generated with

TABLE XI
Air Flow Resistivity and Structure Parameter Information of Webs with Different Sequencing

	Basis weight (kg m^{-2})		Thickness (mm)		Porosity ($1 - \rho_w/\rho_f$)		Massivity (ρ_w/ρ_f)		Air flow resistivity (10^3 Pa s/m^2)	
Fabric	Mean	σ	Mean	σ	Mean	σ	Mean	σ	Mean	σ
PGP	1.57	0.13	12.43	0.27	0.90	0.008	0.10	0.008	47.8	4.2
GPP	1.46	0.11	12.09	1.04	0.91	0.012	0.09	0.012	49.3	10.1
PPG	1.46	0.11	12.09	1.04	0.91	0.012	0.09	0.012	42.8	8.1
PHP	1.35	0.11	12.53	0.66	0.89	0.01	0.11	0.01	37.3	2.60
HPP	1.26	0.07	11.45	0.27	0.92	0.005	0.08	0.005	40.5	9.3
PPH	1.26	0.07	11.45	0.27	0.92	0.005	0.08	0.005	38.3	8.3
LHL	1.32	0.08	12.70	0.29	0.91	0.007	0.09	0.007	25.0	3.7
HLL	1.28	0.07	12.68	0.78	0.91	0.008	0.09	0.008	34.6	11.9
LLH	1.28	0.07	12.68	0.78	0.91	0.008	0.09	0.008	32.8	10.4

an R^2 value of 0.93. Layer sequencing and surface effects were not included in the model as quantitative variables. This might be the reason for the coefficient of determination to be lower than that of eq. (13).

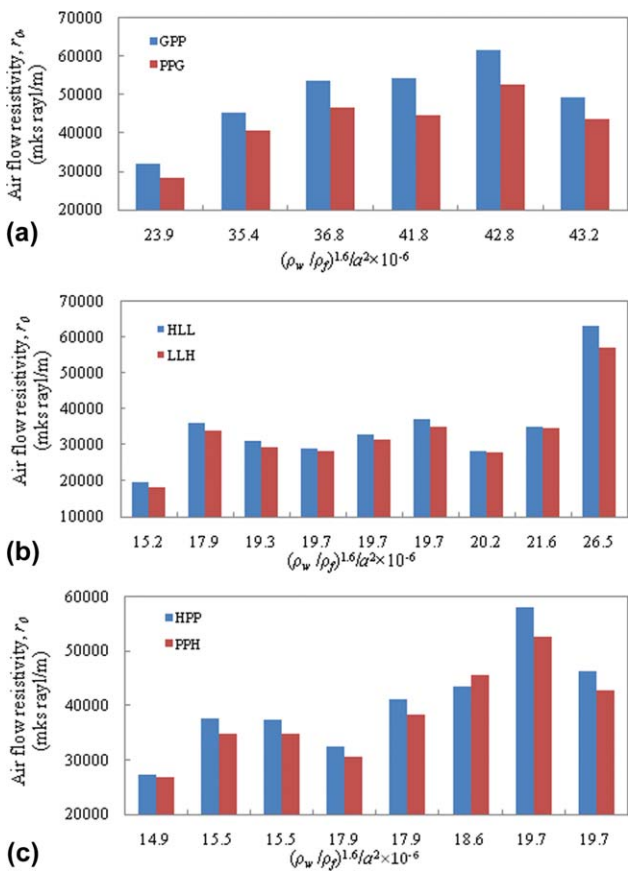

Figure 11 Effect of layer sequencing on air flow resistivity. Comparison of air flow resistivity values of (a) GPP and PPG nonwoven fabrics; (b) HLL and LLH nonwoven fabrics; and (c) HPP and PPH nonwoven fabrics. [Color figure can be viewed in the online issue, which is available at wileyonlinelibrary.com.]

TABLE XII
Difference in Air Flow Resistivity Due to Changing Direction of the Fabric

			Difference in air flow resistivity between sequencing (10^3 Pa s/m^2)		Difference ratio in air flow resistivity between sequencing $[(r_{0f}-r_{0b})/r_{0f}]$[a]	
Fabric	Sequencing		Mean	σ	Mean	σ
GPP	GPP	PPG	6560	2390	0.13	0.03
HPP	HPP	PPH	2130	2250	0.05	0.03
HLL	HLL	LLH	1825	1730	0.05	0.05

[a]Difference ratio in air flow resistivity between sequencing $[(r_{0f}-r_{0b})/r_{0f}]$ is the ratio of the difference between the air flow resistivity value of the fabrics when the reinforcement layer is in the front (r_{0f}) and when it is at the back (r_{0b}) to the value when the reinforcement layer is in the front (r_{0f}).

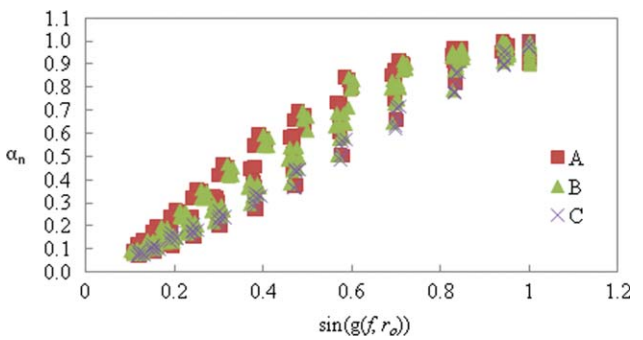

Figure 12 Comparison of statistical model estimates versus actual values for NAC values of different sequenced layered fabrics. X-axis is a function of frequency and air flow resistivity. (A) Reinforcement fiber layer faces the sound source; (B) reinforcement fiber layer is in the middle; and (C), reinforcement fiber layer is at the back. [Color figure can be viewed in the online issue, which is available at wileyonlinelibrary.com.]

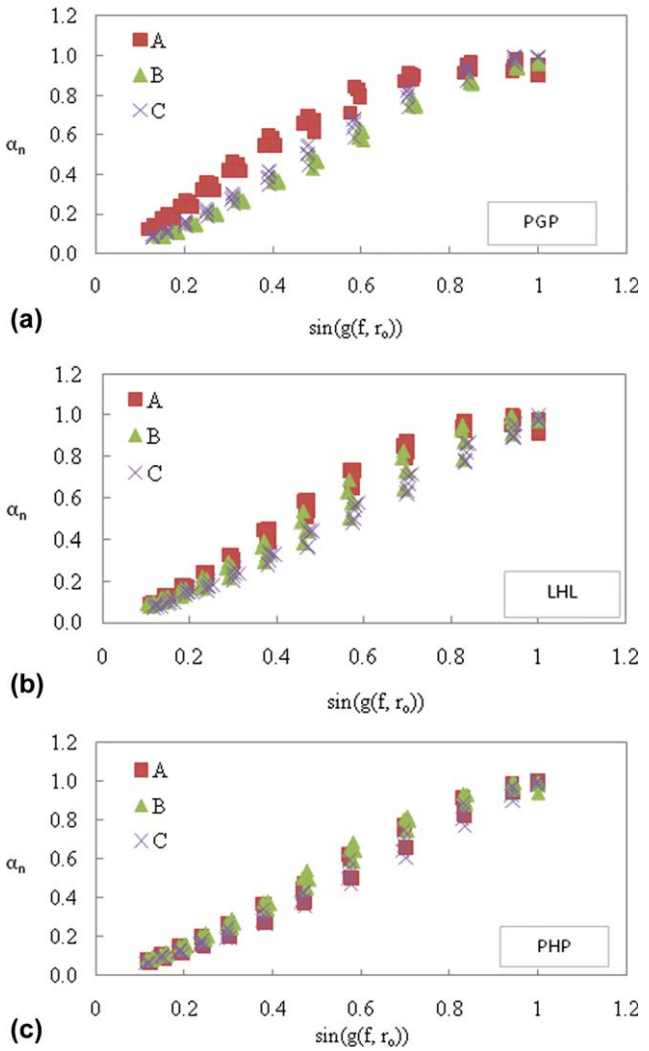

Figure 13 Comparison of statistical model estimates versus actual values for NAC values of different sequenced layered fabrics separately. X-axis is a function of frequency and air flow resistivity. (a) PGP, (b) LHL, and (c) PHP. [Color figure can be viewed in the online issue, which is available at wileyonlinelibrary.com.]

$$\alpha_n = \sin\left(-5.30 \times 10^{-2} + 2.47 \times 10^{-4} f + 1.60 \times 10^{-6} r_0\right) \tag{14}$$

The comparison of the model estimates with experimental results for all fabrics with different layer sequencing is plotted in Figure 12. From the plot, it is seen that the fabrics that had their reinforcement layer at the back (c), tended to have lower NAC values.

In Figure 13(a–c), the sequencing of each of the three fabrics, PGP, PGI, and LHL, can be observed, respectively. In the fabric group PGP, GPP (A) had distinctively higher NAC values than PGP (B) and PPG (C). The difference was still prominent in the fabric group LHL. HLL (A) had higher NAC values than LHL (B), and LLH (C), but not as much as observed in the fabric group PGP. There was very little difference in PHP, HPP, or PPH group, if any. This situation is in agreement with the analysis of the effect of layering sequence on air flow resistance.

CONCLUSIONS

The effects of fiber fineness, porosity, and layer sequencing on air flow resistivity and NAC of single-fiber and multifiber type three-layered nonwoven composites made from PLA, PP, glass fiber, and hemp have been investigated. Air flow resistivity was statistically modeled in terms of porosity and fiber diameter. Results indicate that air flow resistivity increased with decreasing fiber diameter and porosity. An inconsistency was found between the models in the literature that have been developed for glass fiber mats and those that work for the nonwovens studied. A strong relationship between the layering sequence and air flow resistivity was obtained. It was found that when the layer including reinforcement fibers, i.e., hemp or glass fiber, faced the air flow source, the air flow resistance was higher than the case when the layer including reinforcement fibers was farthest away from the air flow source. The difference was more pronounced when there was a higher difference between the resistivity values of the constituent layers of the nonwoven composites. NAC was modeled in terms of air flow resistivity and frequency. Similar to air flow resistivity, NAC was found to be higher when the layer including reinforcement fibers was placed closest to sound source. This finding was more pronounced when there was a higher difference between the resistivity values of the layers.

The authors thank Mr. Michael Hodge from Fiber Innovations, Inc., and Ms. Amy Shuttleworth Vining from AGY for donating fibers, Dr. Behnam Pourdeyhimi of Nonwovens Cooperative Research Center for the nonwoven production, Mr. Gordon Ebbitt from Carcoustics Tech Center for making acoustic testing possible, and Mrs. Carrie Knoebe Houghston for her valuable help in statistical programming.

References

1. Na, Y. J.; Lancaster, J.; Casali, J.; Cho, G. Text Res J 2007, 77, 330.
2. Kondylas, K. Nonwovens Ind 1998, 29, 64.
3. Parikh, D. V.; Parikh, D. V.; Chen, Y.; Sachinvala, N. D. AATCC Rev 2006, 6, 40.
4. McRae, J. D.; Naguip, H. E.; Atalla, N. J Appl Polym Sci 2010, 116, 1106.
5. Ng, Y.-H.; Hong, L. J Appl Polym Sci 2006, 102, 1202.
6. Yilmaz, N. D. Acoustic Properties of Biodegradable Nonwovens. Ph.D. Thesis. North Carolina State University: Raleigh, NC, 2009.

7. Yilmaz, N. D.; Banks-Lee, P.; Powell, N. B. In Proceedings of the INTC 2008 International Nonwovens Technical Conference, Houston, TX, 2008.
8. Cox, T. J.; D'Antonio, P. Acoustic Absorbers and Diffusers; Taylor & Francis: New York, 2004.
9. Fahy, F. Foundations of Engineering Acoustics; Academic Press: San Diego, CA, 2001.
10. Attenborough, K.; Ver, I. L. In Noise and Vibration Control Engineering, 2nd ed.; Ver, I. L., Beranek, L. L., Eds.; Wiley: Hoboken, NJ, 2006; Chapter 8.
11. Delany, M. E.; Bazley, E. N. Appl Acoust 1970, 3, 105.
12. Wang, X. Y.; Gong, R. H. J Appl Polym Sci 2006, 102, 2264.
13. Vitchuli, N.; Shi, Q.; Nowak, J.; McCord, M.; Bourham, M.; Zhang, X. J Appl Polym Sci 2010, 116, 2181.
14. Kan, C. W. J Appl Polym Sci 2008, 107, 1584.
15. American Society for Testing and Materials. ASTM C 522-03. Standard Test Method for Airflow Resistance of Acoustical Materials; ASTM: West Conshohocken, PA, 2008.
16. Bies, D. A.; Hansen, C. H.; Engineering Noise Control: Theory and Practice; Spon Press: New York, 2003.
17. Ballagh, K. O. Appl Acoust 1996, 48, 101.
18. Ingard, K. U. Notes on Sound Absorption Technology; Noise Control Foundation: Poughkeepsie, NY, 1994.
19. Mohammadi, M. Heat Barrier Properties of Heterogeneous Nonwoven Materials. Ph.D. Thesis. North Carolina State University: Raleigh, NC, 1998.
20. Mechel, F. P.; Formulas of Acoustics; Springer: Berlin, Germany, 2002.
21. Kan, C. W.; Yuen, W. M. J Appl Polym Sci 2006, 102, 5958.
22. Drzal, L. T.; Mohanty, D. K.; Burgueno, R.; Misra, M.; In Proceedings of the NSF Housing Research Agenda Workshop, Orlando, FL, February 12–14, 2004.
23. Aziz, S. H.; Ansell, M. P. In Green Composites; Baillie, C., Ed.; Woodhead Publishing: Cambridge, 2004; Chapter 8.
24. Olesen, P. O.; Plackett, D. V. In Proceedings of the Natural Fibres Performance Forum, Copenhagen, Denmark, May 27–28, 1999.
25. Bismarck, A.; Mishra, S.; Lampke, T. In Natural Fibers, Biopolymers, and Biocomposites; Mohanty, A. K., Misra, M., Drzal, L. T., Eds.; Taylor & Francis: Boca Raton, FL, 2005; Chapter 2.
26. American Society for Testing and Materials. ASTM D 1577 07. Standard Test Methods for Linear Density of Textile Fibers; ASTM: West Conshohocken, PA, 2007.
27. American Society for Testing and Materials. ASTM D 3776 07. Standard Test Methods for Mass Per Unit Area (Weight) of Fabric; ASTM: West Conshohocken, PA, 2007.
28. American Society for Testing and Materials. ASTM D 5729-97. Standard Test Method for Thickness of Nonwoven Fabrics; ASTM: West Conshohocken, PA, 1997.
29. American Society for Testing and Materials. ASTM C 830-00. Standard Test Methods for Apparent Porosity, Liquid Absorption, Apparent Specific Gravity, and Bulk Density of Refractory Shapes by Vacuum Pressure; ASTM: West Conshohocken, PA, 2000.
30. American Society for Testing and Materials. ASTM D 737-04. Standard Test Method for Air Permeability of Textile Fabrics; ASTM: West Conshohocken, PA, 2004.
31. Frazier Precision Instrument Company, Inc. Frequently Asked Questions about the Frazier Differential Pressure Air Permeability Instrument. 2009. Available at: http://www.frazierinstrument.com/products/fap/fap-faq.html. Accessed December 3, 2009.
32. American Society for Testing and Materials. ASTM E 1050-07. Standard Test Method for Impedance and Absorption of Acoustical Materials Using a Tube, Two Microphones and a Digital Frequency Analysis System; ASTM: West Conshohocken, PA, 2007.
33. Bruel & Kjaer. Product Data Impedance Tube Kit (50 Hz-6.4 kHz)—Type 4206. 2009. Available at: http://www.bksv.com/doc/Bp1039.pdf. Accessed December 3, 2009.
34. Bies, D. A.; Hansen, C. H. Appl Acoust 1980, 13, 357.
35. Garai, M.; Pompoli, F. In Proceedings of Forum Acusticum, Sevilla, 2002; RBA-03-004-IP.